Further Discoveries of ^{12}CO in Low Surface Brightness Galaxies

K. O'Neil
NAIC/Arecibo Observatory, HC3 Box 53995, Arecibo, PR 00612 USA
koneil@naic.edu

E. Schinnerer[1]
Jansky Fellow; NRAO, P.O. Box 0, Socorro, NM 87801 USA
eschinne@nrao.edu
and

P. Hofner
Physics Department, U. of Puerto Rico at Rio Piedras, P.O. Box 23343, San Juan, PR 00931 USA
NAIC/Arecibo Observatory, HC3 Box 53995, Arecibo, PR 00612 USA
hofner@naic.edu

ABSTRACT

Using the IRAM 30m telescope we have obtained seven new, deep CO J(1−0) and J(2−1) observations of low surface brightness (LSB) galaxies. Five of the galaxies have no CO detected to extremely low limits (0.1 – 0.4 K km s^{-1} at J(1−0)), while two of the galaxies, UGC 01922 and UGC 12289, have clear detections in both line transitions. When these observations are combined with all previous CO observations taken of LSB systems, we compile a total of 34 observations, in which only 3 galaxies have had detections of their molecular gas. Comparing the LSB galaxies with and without CO detections to a sample of high surface brightness (HSB) galaxies with CO observations indicates that it is primarily the low density of baryonic matter within LSB galaxies which is causing their low CO fluxes. Finally, we note that one of the massive LSB galaxies studied in this project, UGC 06968 (a Malin-1 'cousin'), has upper limits placed on both M_{H_2} and M_{H_2}/M_{HI} which are 10–20 times lower than the *lowest* values found for any galaxy (LSB or HSB) with similar global properties. This may be due to an extremely low temperature and metallicity within UGC 06968, or simply due to the CO distribution within the galaxy being too diffuse to be detected by the IRAM beam.

Subject headings: Galaxies: CO,H_2 — Galaxies: ISM — Galaxies: low surface brightness — Galaxies: spiral — Galaxies: evolution

1. Introduction

Despite more than a decade of study, the star formation processes within low surface brightness (LSB) galaxies remain enigmatic. The general properties of LSB galaxies – blue colors, high gas mass-to-luminosity ratios, and low metallicities – lead to the conclusion that LSB systems are under-evolved compared to their high surface brightness (HSB) counterparts. When combined with the low gas density (typically $\rho_{\rm HI} \leq 10^{21}$ cm^{-2}) and low baryonic-to-dark matter content typical of LSB systems, the question can be raised not of why LSB galaxies are under-evolved, but instead of how LSB systems ever form stars at all (Burkholder, Impey, & Sprayberry 2001; O'Neil, Bothun, & Schombert 2000; Bergvall, et.al 1999; de Blok & van der Hulst 1998; Roennback & Bergvall 1995; McGaugh 1994; van der Hulst, et.al 1993; Davies, Phillipps, & Disney 1990).

One of the primary methods for studying the star formation rate and efficiency in galaxies is through study of the galaxies' ISM. One mechanism for studying a galaxy's ISM is through observing its CO content. Numerous attempts have been made looking for CO in LSB systems without success (Braine, Herpin, & Radford 2000; de Blok & van der Hulst 1998; Schombert, et.al 1990). If CO is as good a tracer of H_2 in LSB galaxies as it is in many HSB systems, the failures in detecting CO would imply a lack of molecular gas within LSB galaxies. Alternatively, the previous non-detections could be a result of a CO-to-H_2 ratio which is different in LSB systems than in, e.g. the Milky Way. However, without any CO detections within LSB systems discerning between the two possibilities is difficult, if not impossible.

Recently our group made the first CO detection in an LSB galaxy ([OBC97] P06-1) (O'Neil, Hofner, & Schinnerer 2000). Significant though this detection is, knowing the molecular content of one galaxy is not enough to permit an understanding of the star formation within LSB systems as a whole. Emboldened by the success of our earlier survey, and wishing to obtain a larger sample of CO measurements within LSB galaxies, we have observed another set of seven LSB galaxies with the IRAM 30m telescope to look for the CO J$(1-0)$ and J$(2-1)$ lines. The results of our survey are presented here. In order to understand better the molecular properties of LSB galaxies as a whole, we also include the results of all previously published CO observations of LSB systems and compare the molecular properties of LSB galaxies with those of similar HSB systems.

A Hubble constant of H_0=75 km s^{-1} Mpc^{-1} is assumed throughout this paper.

2. Observations

2.1. CO

Based off previous observations of CO in LSB galaxies, we chose to look for evidence of molecular gas in LSB systems similar to the global properties of [OBC97] P06-1, the one LSB galaxy with a CO detection (O'Neil, Hofner, & Schinnerer 2000). Comparing the properties of P06-1 with the other LSB galaxies observed at CO, it is clear that P06-1 is one of the more massive systems studied ($\log(M_{HI}/M_\odot) = 10$, $W_{20} = 460$ km s^{-1}– Table 2), and also one whose optical spectra indicates some nuclear activity (Section 3.2). With this in mind, we chose to focus the observations on massive LSB systems, some with and some without AGN/LINER characteristics. The galaxies for this sample were chosen from three separate sources – the massive LSB galaxy catalog of O'Neil, et.al (2003), the AGN LSB list provided in Schombert (1998)

[1]Work done while at California Institute of Technology

TABLE 1
SOURCES OBSERVED IN CO

Name	RA [J2000]	DEC [J2000]	Int. Time [min]	σ_{rms}^{1-0} [mK]	σ_{rms}^{2-1} [km s^{-1}]	Res.† [mK]	Set-up‡
UGC 01922	02:27:46.01	28:12:30.3	730	0.7	0.8	33	B
[OBC97] C04-1	08:24:33.19	21:27:07.8	310	1.1	2.5	33	B
[OBC97] N09-2	10:20:25.01	28:13:40.9	440	1.2	2.0	26	A
UGC 06968	11:58:44.63	28:17:23.2	690	0.5	1.5	33	B
UGC 12289	22:59:41.59	24:04:28.5	360	0.9	1.0	33	B
[OBC97] P05-6	23:21:46.97	09:02:28.5	640	0.7	1.3	26	A
[OBC97] P07-1	23:22:58.87	07:40:26.7	480	0.9	1.2	26	A

NOTE.—†Smoothed resolution used for data analysis.
‡See Section 2.1 for a description of the backend set-ups.

of LSB galaxies with AGN/LINER cores, and the LSB galaxy catalog of O'Neil, Bothun, & Schombert (2000). A full list of the galaxies observed and their properties are given in Tables 1 and 2, and the results of the observations are given in Table 3. The resultant spectra are shown in Figures 1 and 2.

The CO J(1–0) and J(2–1) rotational transitions were observed with the IRAM 30m telescope in the period from 25-28 May, 2001. Table 1 lists the adopted positions (determined using the digitized Palomar sky survey plates and accurate to 2-3″) and heliocentric velocities (adopted from the published values obtained from 21-cm HI observations) for our target sources. The beams were centered on the nucleus of each galaxy. Pointing and focus were checked every hour and pointing was found to be better than 5″. For each source both transitions were observed simultaneously with two receivers. Two different setups were used for the filterbanks, depending upon the known HI line widths of the individual galaxy. For those galaxies known to have HI line widths less than 300 km s^{-1} both receivers used a 256 channel filterbank with channel width of 3 MHz (667 km s^{-1} bandwidth, 2.6 km s^{-1} resolution at 3mm) – setup A. For the sources which are known to have wider HI lines the 1mm lines used a 512 channel filter bank with 1 MHz channels for each polarizations, while the 3mm line used the auto-correlator with 512 MHz bandwidth and 1MHz channels (1331 km s^{-1} bandwidth, 2.6 km s^{-1} resolution at 3mm) – setup B. Table 1 gives the set-up used for the individual galaxies. The FWHM of the IRAM beam is 22″ and 11″ for the 3mm and 1mm beams, respectively.

All observations used the wobbling secondary with the maximal beam throw of 240″. The image side band rejection ratios were measured to be $>$ 30dB for the 3 mm SIS receivers and $>$ 12dB for the 1.3 mm SIS receivers. The data were calibrated using the standard chopper wheel technique (Kutner & Ulich 1981) and are reported in main beam brightness temperature T$_{MB}$. Typical

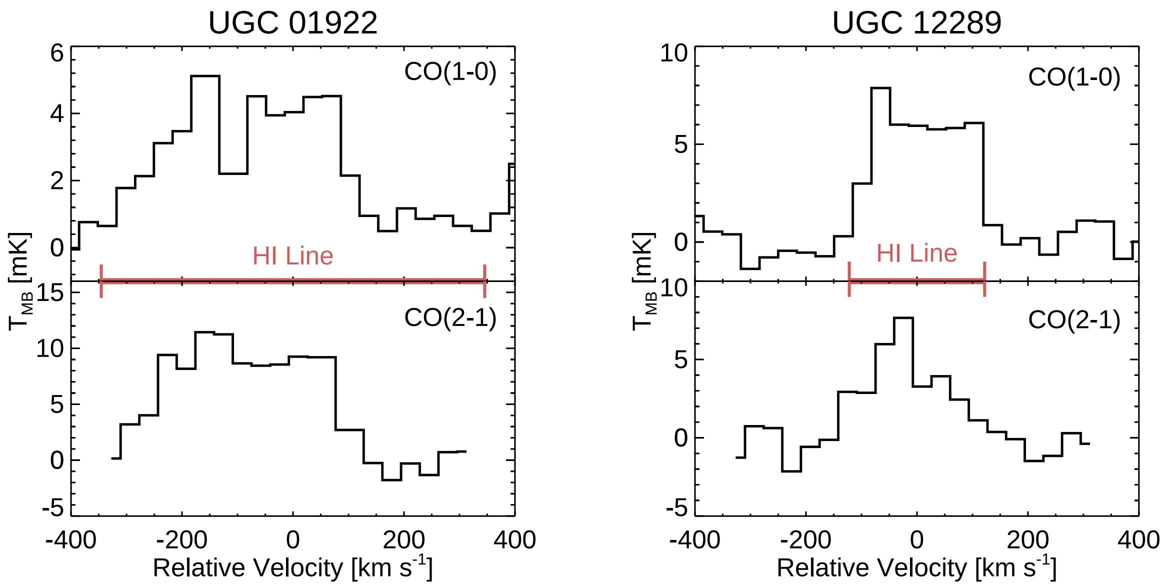

Fig. 1.— IRAM 30m CO J(1−0) and J(2−1) spectra for UGC 01922 (left) and UGC 12289 (right), the two galaxies in this survey with detectable amounts of molecular gas. The data have been smoothed to a resolution of 34 $\mathrm{km\,s^{-1}}$. The horizontal bars indicate the extent of the observed (uncorrected) H I velocity widths (at 20% the peak HI intensity).

system temperatures during the observations were 170–190K and 350–450K in the 3 mm and 1.3 mm band, respectively. All data reduction was done using CLASS – the Continuum and Line Analysis Single-dish Software developed by the Observatoire de Grenoble and IRAM (Buisson, et.al 2002).

2.2. Optical Spectra

In order to further explore the properties of the studied galaxies' nuclear regions (where the IRAM beam was centered), optical spectra of the nuclei of a sample of LSB galaxies which have been observed in CO were taken with the Palomar Observatory 5m telescope[2] in October 2000 (the [OBC97] galaxies) and November 2001 (the UGC galaxies).

[2]Observations at the Palomar Observatory were made as a part of the cooperative agreement between Cornell University and the California Institute of Technology

The observations used the Double Spectrograph with both the blue and red cameras. The long slit (2′) was used and set to a 2" aperture during all observations. Both cameras are 1024×1024 TEK CCD cameras, giving 3.37Å pixel^{-1}/0.624″ pixel^{-1} and 2.48Å pixel^{-1}/0.48″ pixel^{-1} for the blue and red cameras, respectively. As the blue CCD has moderate focusing problems across the full wavelength range, the blue focus was optimized for [O III]λ3727.

During the October 2000 run a 5500Å dichroic filter was used to split the light to the blue and red CCD cameras. A 316 lines mm^{-1} diffraction grating (blazed at 7150Å) was used for the red camera and the 300 lines mm^{-1} diffraction grating (blazed at 3990Å) was used for the blue camera during this run. In November 2001 the 5200 Å dichroic filter was used with the 600 lines mm^{-1} diffraction grating (blazed at 3780Å) on the blue camera

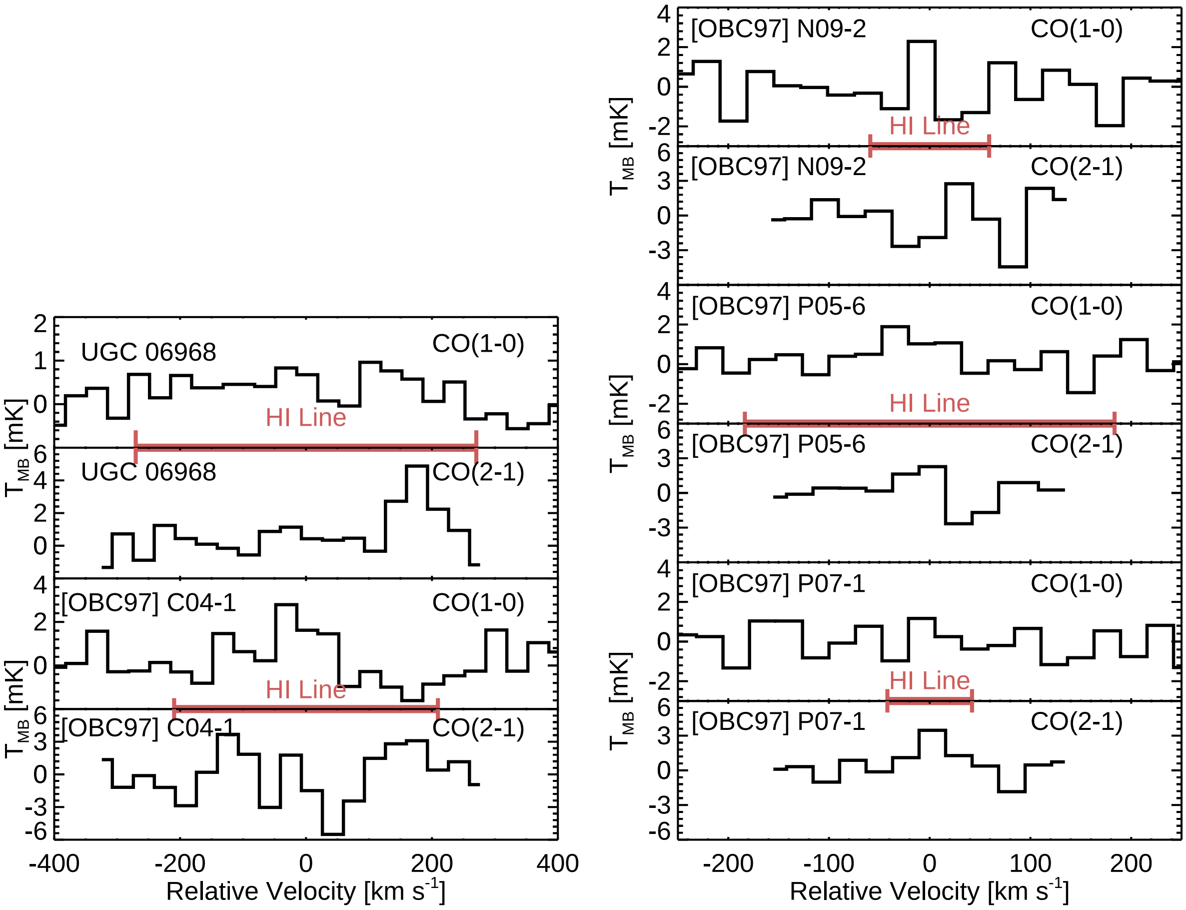

Fig. 2.— IRAM 30m CO J(1−0) and J(2−1) spectra for the five galaxies in our survey for which we derived only upper limits on the CO line strengths. The data have been smoothed to a resolution of 34 km s^{-1}. The horizontal bars indicate the extent of the observed (uncorrected) H I velocity widths (at 20% the peak HI intensity).

and the 316 lines mm^{-1} diffraction grating (blazed at 7150Å) on the red camera. The seeing averaged between 1.5 – 2.1$''$ for the observations.

The galaxies were acquired through blind offsets from nearby stars. Positions were obtained through a combination of both the HST Guide Star Catalog and the second generation Palomar Survey Data. Based off the studies of van Zee, et.al (1998) offsets were kept to less than 20$'$ and guide stars were chosen to have m$_B$<11 to insure accurate offsets and guiding. To reduce light losses due to atmospheric refraction, the slit position angle was set close to the parallactic angle during observations. The slits were placed across the nucleus of each galaxy. The integration times were 1200s per frame. The total (on source) observing times were 120, 260, 220, 300, 80, and 120 minutes for [OBC97] C04-2, [OBC97] P05-5, [OBC97] P05-6, [OBC97] P06-1, UGC 01922, and UGC 12289, respectively.

The standard IRAF data reduction pro-

Table 2
Known Properties of All LSB Galaxies Observed at CO

Name	Type	$\mu_B(0)$ [mag arcsec^{-2}]	B_T[a] [mag]	D[a] [kpc]	B−V	i [°]	$\log(\frac{L_{FIR}}{L_\odot})$[b]	$\log(\frac{M_{HI}}{M_\odot})$	v^{HI}_{HEL} [km s^{-1}]	$w^{HI}_{20_{cor}}$[c] [km s^{-1}]
Detections – This Paper										
UGC 01922	S?[1]	…[d]	-19.8	59	…	38[2]	10.6	10.33[3]	10894[3]	1120[3]
UGC 12289	Sd[1]	23.3[4]	-19.7	57	…	22[2]	10.7	10.13[3]	10160[3]	488[3]
Previous Detection										
[OBC97] P06-1	Sd[5]	23.2[6]	-18.6	29	0.9[7]	70[6]	<10.2	9.87[5]	10882[5]	458[5]
Non-Detections – This Paper										
[OBC97] P07-1	Sc[5]	23.3[6]	-16.3	16	…	75[6]	<9.4	8.21[5]	3471[5]	87[5]
[OBC97] N09-2	Im[5]	23.5[6]	-16.2	13	0.8[7]	47[6]	<9.7	10.03[5]	7746[5]	161[5]
[OBC97] P05-6	Sbc[5]	23.4[6]	-16.5	17	0.7[7]	75[6]	<9.3	9.24[5]	3667[5]	380[5]
[OBC97] C04-1	Im[5]	23.4[6]	-17.3	14	0.5[7]	39[6]	<9.9	9.74[5]	7905[5]	419[5]
UGC 06968	Sc[1]	…[d]	-21.1	48	1.0[8]	71[2]	<9.8	10.30[9]	8232[9]	574[9]
Previous Non-Detections										
LSBC D575-05	dI[10]	(22.5)[e]	-12.2	2.0	…	60[11]	<7.2	7.47[12]	419[12]	27[12]
LSBC F571-V2	Im[13]	…	…	3.3	…	37[10]	<7.8	8.06[14]	955[14]	53[14]
LSBC F638-3	Sm[15]	…	-16.4	6.1	…	46[11]	<8.9	8.88[15]	3160[15]	58[15]
LSBC F583-5	Sm[10]	23.5[16]	-14.7	24	0.6[16]	65[16]	<8.9	9.11[17]	3261[17]	28[17]
LSBC F651-2	dI[15]	…	-15.5	4.9	…	46[11]	<8.3	8.73[15]	1789[15]	70[15]
LSBC F721-1	Sdm[15]	…	-18.9	17	…	41[11]	<9.7	9.52[15]	7210[15]	98[15]
LSBC F571-V1	Im[15]	24.0[18]	-15.9	20	0.4[18]	35[18]	<9.5	9.07[15]	5719[15]	113[15]
[OBC97] P05-5	Im[5]	24.4[6]	-14.5	5.7	1.2[7]	49[6]	<9.1	7.78[5]	3177[6]	94[6]
LSBC F636-1	Sm(r)[15]	…	-17.5	13	…	52[11]	<9.3	9.27[15]	4302[15]	95[15]
LSBC F562-V2	S:[10]	…	-18.1	12	…	20[10]	<9.4	9.59[15]	6330[15]	156[15]
LSBC F563-V1	Im[15]	23.4[18]	-15.8	6.1	0.6[18]	60[18]	<9.3	8.73[15]	3931[15]	90[15]
LSBC F561-1	Sm[15]	23.2[18]	-17.5	19	0.5[18]	24[18]	<9.4	8.81[15]	4810[15]	160[15]
LSBC F574-10	Sm[10]	…	-12.8	3.0	…	72[10]	<7.8	8.23[15]	863[15]	86[15]
LSBC F585-V1	dI[15]	23.4[16]	-13.7	3.1	…	41[15]	<8.5	8.11[13]	1985[13]	126[13]
[OBC97] C04-2	Im[5]	24.0[6]	-16.5	13	1.3[7]	67[6]	<9.5	8.82[5]	5168[5]	111[5]
LSBC F563-V2	Irr[15]	22.0[16]	-17.3	15	0.5[16]	40[16]	<9.2	9.31[15]	4311[15]	184[15]
LSBC F563-1	Im[15]	23.6[18]	-16.6	14	0.9[18]	25[18]	<9.0	9.04[14]	3495[14]	252[14]
LSBC F571-5	Sm[15]	23.7[18]	-16.0	17	0.3[18]	26[18]	<9.3	9.24[15]	4253[15]	260[15]
[OBC97] C05-3	Im[5]	23.9[6]	-17.3	20	1.3[7]	51[6]	<10.0	9.41[5]	12940[5]	167[5]
LSBC F585-3	Sm[15]	…	-16.5	13	…	74[10]	<9.0	9.20[13]	3100[13]	154[13]
LSBC F568-V1	Sc[15]	23.2[18]	-17.2	16	0.6[18]	40[18]	<9.5	9.39[15]	5768[15]	249[15]
LSBC F583-1	Sm/Irr[15]	24.1[19]	-15.9[14]	8.8	…	63[19]	<8.7	9.18[15]	2264[15]	181[15]
LSBC F582-V1	Ring[10]	…	-18.0	9.1	…	20[10]	<10.0	9.85[15]	11695[15]	356[15]
LSBC F564-V2	Im[15]	…	…	9.5	…	29[10]	<9.0	8.91[13]	3060[13]	358[13]
LSBC F582-2	Sbc[15]	…	…	41	…	66[10]	<9.6	9.99[15]	7043[15]	310[15]
Malin 1	S[20]	26.4[20]	-21.4[20]	240	0.9[20]	20[20]	<11.0	10.6[20]	24733[20]	710[20]

Note.— [a]Unless otherwise noted magnitudes and diameters are taken from NED, the NASA Extragalactic Database. [b]FIR luminosities are given by $\log(L_{FIR}) = 46.73 + 2log[z(1+z)] + log[2.58f_{60} + f_{100}]$ where f_{60} and f_{100} are in Jy and L_{FIR} is in erg s^{-1}. Fluxes were obtained from the Infrared Astronomical Satellite (IRAS) data. [c]Velocity widths are corrected for inclination using $w^{HI}_{20_{corr}} = w^{HI}_{20}/sin\ i$. To avoid over-correcting the velocity widths, the smallest inclination value used for the purpose of correcting the velocity widths is 30°. [d]The classification of this galaxy as an LSB galaxy is from Schombert (1998). [e]The reported central surface brightness is through the V (not B) band (Pildis, Schombert, & Eder 1997).

References.— [1] Schombert (1998); [2] Nilson (1973); [3] Giovanelli & Haynes (1985); [4] Data taken with the Pine Mountain Observatory telescope. PMO is operated by the University of Oregon Physics Department with help from the Friends of Pine Mountain Observatory. Image obtained courtesy of G. Bothun.; [5] O'Neil, Bothun, & Schombert (2000); [6] O'Neil, Bothun, & Cornell (1997a); [7] O'Neil, et.al (1997b); [8] Boselli & Gavazzi (1994); [9] Gavazzi (1987); [10] Schombert & Bothun (1988); [11] Garnier, et.al (1996); [12] Eder & Schombert (2000); [13] Schombert, et.al (1990); [14] de Blok, McGaugh, & van der Hulst (1996); [15] Schombert, et.al (1992); [16] McGaugh & Bothun (1994); [17] Huchtmeier, Karachentsev, Karachentseva (2000); [18] de Blok, van der Hulst & Bothun (1995); [19] de Blok & McGaugh (1997); [20] Impey & Bothun (1989) cedures as outlined in, e.g. van Zee, et.al (1998), were followed. Each frame individually underwent bias subtraction and flatfielding. Frames of the same source and taken on the same night were median combined. The resultant image then underwent sky subtraction and wavelength and photometric calibration. Images of the same object taken at different times were then combined (using IRAF's SCOMBINE procedure), and extinction and foreground reddenning due to our Galaxy was corrected. Wavelength calibration was obtained by observation of arc lamps taken before and after each galaxy observation. A hollow cathode (FeAr) lamp was used to calibrate the blue wavelengths, and a HeNeAr lamp was used to calibrate the red camera. Flux calibration was obtained by observation of a minimum two standard stars each night (Oke & Gunn 1983; Oke 1990; Massey, et.al 1988). Extinction correction was done based off the KPNO extinction table given for IRAF's ONEDSPEC routine. Galactic extinction was corrected for using the reddening law of Seaton (1979) as parameterized by Howarth (1983). Values for A_B and E(B-V) are from Schlegel, Finkbeiner, & Davis (1998) and were obtained using NED (the NASA Extragalactic Database)[3].

Errors were determined as follows. Flux calibration errors, due primarily to differences in the standard star calibrations, were consistently less than 10%. The r.m.s. errors varied with wavelength across the spectra due to CCD response, calibration lamp accuracy, etc. Rms errors were determined through taking into account the Poisson noise of the line, the error associated with the sensitivity function, read noise, and sky noise. Note that no error was assumed for the effects of the assumed Balmer absorption or the reddening coefficient.

Results from the optical observations are shown in Figures 3 and 4 and Table 4.

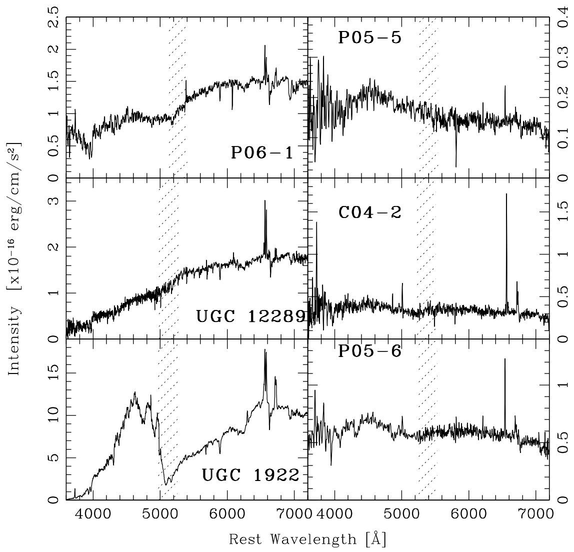

Fig. 3.— Uncorrected optical spectra taken by the Palomar 5m telescope for a sample of LSB galaxies with studied CO properties. The diagonal lines mark the boundary where the dichroic filter transmission falls by ≥20% for each camera and the data should not be trusted within that region. The three LSB galaxies with detected CO emission are on the left, while three LSB galaxies with no detectable molecular gas are on the right. Note that the underlying shape of UGC 01922's spectra is likely due to SN1987s which occurred approximately 40″ from the galaxy's center (O'Neil & Schinnerer 2003).

3. Results

3.1. CO Observations

The results of our CO observations are given in Table 3 and Figures 1 and 2. Of the seven galaxies observed for this project, CO was detected in only two – UGC 01922 and UGC 12289. Both detected galaxies have

[3]NED is operated by the Jet Propulsion Laboratory, California Institute of Technology, under contract with NASA.

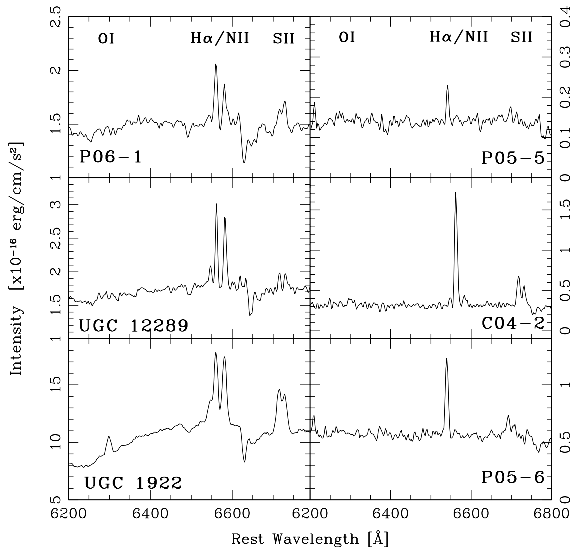

Fig. 4.— Blow-up on the [O I], [N II], Hα, and [S II] region of the optical spectra. As in Figure 3, the three LSB galaxies with detected CO emission are on the left, while three LSB galaxies with no detectable molecular gas are on the right.

clear (5–6σ) detections in the J(1–0) line and a $\geq 4\sigma$ detection in the J(2–1) line. After smoothing to 34 $\mathrm{km\,s^{-1}}$ channel^{-1}, the observed main beam brightness temperature was 3.4±0.7/7.3±0.8 mK and 5.8±0.9/3.5±1.0 mK for the J(1–0)/J(2–1) lines of UGC 01922 and UGC 12289, respectively. The galaxies have fluxes of 1.38±0.30/2.96±0.32 K $\mathrm{km\,s^{-1}}$ and 1.16±0.27/0.69±0.23 K $\mathrm{km\,s^{-1}}$ for UGC 01922 and UGC 12289, respectively. (Errors for the flux are computed from the r.m.s. error of the main beam brightness temperature and an assumed 34 $\mathrm{km\,s^{-1}}$ error for the velocity width.)

The 3σ non-detection limits for the five galaxies without CO detections range between 1.5 – 3.6 mK. These detection limits are similar to those found by O'Neil, Hofner, & Schinnerer (2000), and are a factor of 6-7 times smaller than the CO studies on LSB galaxies done by both de Blok & van der Hulst (1998) and Schombert, et.al (1990). The integrated flux limits, though, are only slightly smaller than those in the de Blok & van der Hulst (1998) study due to smaller total mass (narrower velocity widths) of their sample.

The apparent optical diameters of the galaxies in this study range from $0.4'$ – $2.8'$ (Table 2), while the beam size of the IRAM telescope is $11''$ and $22''$ for the J(2–1) and J(1–0) lines, respectively. Using 2.6-mm CO observations of more than 200 high surface brightness (HSB) spiral galaxies, Young, et.al (1995) found the average extent of CO gas in the studied galaxies are one-half the optical radius. If this trend holds true for LSB galaxies, it would indicate the IRAM beam enclosed the entire (potential) reservoir of CO gas only for [OBC97] N09-2, while the other galaxies had 50% (UGC 12289, [OBC97] P07-1, [OBC97] P05-6) and 35% (UGC 01922, UGC 06968) of their potential CO radius enclosed by the J(1–0) beam. However, a recently obtained synthesis map of the CO J(1−0) emission of UGC 01922 obtained with the Owens Valley Radio Observatory millimeter-wavelength array shows Young, et.al's findings may not be applicable to LSB systems. Approximately 65% of the flux found with the IRAM 30m telescope was detected at OVRO within a $\sim 10''$ disk. This shows that at least in UGC 01922 the CO emission is dominated by a brighter compact nuclear region (which would readily fall within the IRAM beam), rather than consisting solely of a large-scale diffuse (low surface density) disk.

The integrated CO flux (or upper limits) of the observed galaxies were converted into an H_2 mass by assuming a value of $\mathrm{N(H_2)}/\int \mathrm{T(CO)dv} = 3.6 \times 10^{20}\ \mathrm{cm^{-2}/(K\ km\ s^{-1})}$ adopted from Sanders, et.al (1986). It has often been argued that the CO $\leftrightarrow$ H_2 conversion factor (X) varies with ISM density structure, metallicity and H I column density (Mihos, Spaans, & McGaugh 1999; Isreal 1997; Wilson 1995; Maloney & Black 1998). If this is the case, then the X factor used in our calculations could be low by as much as a factor of 10 (Mihos, Spaans, & McGaugh 1999). Regardless, to allow for a ready comparison between the objects, the X factor used for our data analysis is the same as that used in both all previous LSB galaxy CO studies as well as in all other CO studies discussed in this paper. Errors due to this assumption are discussed later in this paper (Section 5).

3.2. Optical Spectra

Looking at both Table 4 and Figure 3, the spectra appear to fall into two categories – systems containing both a significant number of absorption lines as well as high [N II/Hα] ratios, and those spectra devoid of absorption lines and containing [N II/Hα] ratios typical of a younger stellar population. Significantly, this breaking of the optical spectra into two distinct groups coincides with the detection (or lack thereof) of molecular gas in the galaxies. That is, the three galaxies which have detectable amounts of CO also have optical spectra indicative of an older stellar population with a potential AGN/LINER core, while the galaxies without any discernable molecular gas appear to have a young overall stellar age with no indication of any high-energy star-formation activity within the galaxies' cores. Note that the underlying shape of UGC 01922's spectra is likely due to SN1987s which occurred approximately 40$''$ from the galaxy's center (O'Neil & Schinnerer 2003).

4. Comparison with Other Galaxies

Combining all CO observations taken of LSB galaxies provides us with a compendium of 34 galaxies, three of which have been detected at both CO J(1–0) and J(2–1). Although this is by no means a statistically complete sample, it is enough to at least try and understand the molecular gas content within these enigmatic systems.

4.1. Finding CO in LSB Galaxies

In Tables 2 and 3 we compile a list of the global properties of all LSB galaxies which have (published) CO observations. Looking through the tables it can be seen that the galaxies with CO detections ("CO LSB galaxies") are not distinguished from the non-detections ("non-CO LSB galaxies") by their morphological type, central surface brightness, inclinations, or color (in the one case of a CO LSB galaxies with a measured $B-V$ color). The only distinguishing feature among the CO LSB galaxies is an apparent higher-than-average size and mass. That is, the absolute magnitudes, H I gas mass, optical diameter, and total mass (as defined by the inclination corrected velocity widths) are on average considerably higher for the CO LSB galaxies than for the non-CO LSB galaxies (Figures 5 & 6).

A second factor which sets the CO LSB galaxies apart the majority of the non-detections is the presence of an extremely active central region (e.g. LINER/AGN). Eight LSB galaxies have both CO observations and optical spectra taken across the galaxy's core. (The two optical spectra not given in this paper can be found in Schombert (1998) – UGC 06968, and Braine, Herpin, & Radford (2000) – Malin 1.) Out of these, all three of the CO LSB galaxies have high N II/Hα line ratios, while only two of the five non-CO LSB galaxies (UGC 06968 and Malin 1) show this. Additionally, both of the CO LSB galaxies covered by 2MASS[4] have

[4]2MASS, the Two Micron All Sky Survey is a joint project of the University of Massachusetts and the Infrared Processing and Analysis Center/California In-

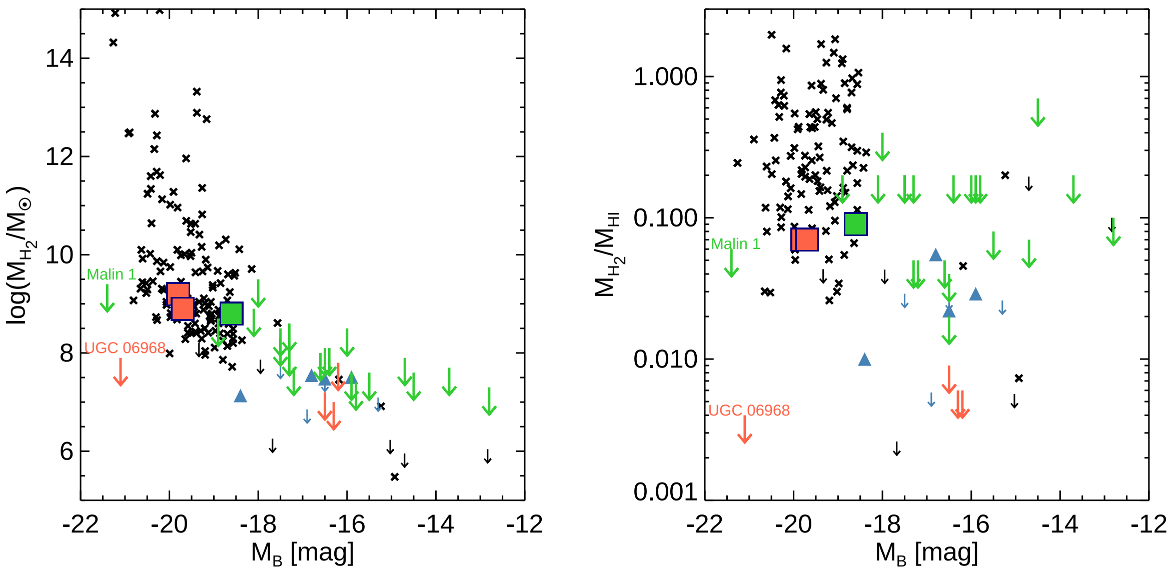

Fig. 5.— Absolute (B) magnitude versus H_2 mass (left) and the H_2-to-H I mass ratio (right). The red symbols are LSB galaxies from this survey, the green symbols are LSB galaxy measurements from previous surveys (O'Neil, et.al 2003; Braine, Herpin, & Radford 2000; de Blok & van der Hulst 1998; Schombert, et.al 1990), the blue symbols are from the Matthews & Gao (2001) study of CO in extreme late-type spiral galaxies, and the black symbols are taken from various studies of the CO content in HSB spiral galaxies (Casoli, et.al 1996; Boselli, et.al 1996; Tacconi & Young 1987). Note that the two LSB galaxy detections from this survey are overlapping in the figure on the right. An arrow indicates only an upper limit was found. Both Malin 1 and UGC 06968, the two massive LSB galaxies discussed in Section 5.3, are labelled on these plots.

entries in the 2MASS extended source catalog (UGC 01922: J=11.60±0.02, H=10.80±0.02, K_s=10.47±0.02; UGC 12289: J=13.30±0.05, H=12.60±0.06, K_s=12,24±0.07), while only two of the remaining 27 non-CO LSB galaxies covered by published 2MASS data are in the catalog (UGC 06968: J=12.45±0.02, H=11.69±0.02, K_s=11.50±0.03; Malin 1: J=14.54±0.06, H=13.83±0.08, K_s=13.7±0.1). Combined, these results suggest the CO LSB galaxies have more active nuclear regions than the non-CO LSB galaxies.

stitute of Technology, funded by the National Aeronautics and Space Administration and the National Science Foundation.

LSB galaxies with detectable quantities of CO appear to have both high masses/sizes and more active nuclear regions than the non-CO LSB systems. Yet even the combination of these two quantities does not guarantee that an LSB system will be detectable in CO. Both UGC 06968 and (of course) Malin 1 have velocity widths and absolute magnitudes to rival those of the three CO LSB galaxies and similar optical spectra, yet neither of these two galaxies have detectable quantities of CO to very low limits ($\int_{CO(1-0)} T_{MB} dv$ <0.21, 0.15 K km s^{-1} and $\log(M_{H_2}/M_\odot)$ <7.9, 9.4 for UGC 06968 and Malin 1, respectively). As a result, although it would appear that having a high mass and active nucleus raises

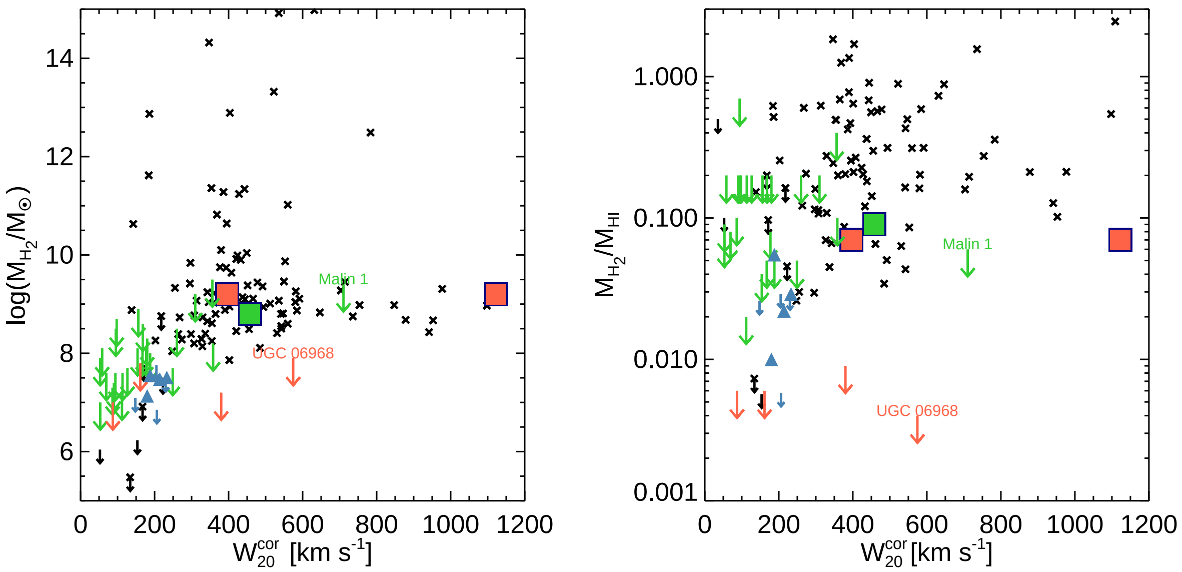

Fig. 6.— Inclination corrected H I velocity widths versus H_2 mass (left) and the H_2-to-H I mass ratio (right). The red symbols are LSB galaxies from this survey, the green symbols are LSB galaxy measurements from previous surveys (O'Neil, et.al 2003; Braine, Herpin, & Radford 2000; de Blok & van der Hulst 1998; Schombert, et.al 1990), the blue symbols are from the Matthews & Gao (2001) study of CO in extreme late-type spiral galaxies, and the black symbols are taken from various studies of the CO content in HSB spiral galaxies (Casoli, et.al 1996; Boselli, et.al 1996; Tacconi & Young 1987). An arrow indicates only an upper limit was found. Both Malin 1 and UGC 06968, the two massive LSB galaxies discussed in Section 5.3, are labelled on these plots.

the probability of an LSB galaxy containing a detectable amount of CO, high mass by no means guarantees a galaxy will have sufficient CO content for detection.

4.2. Comparing the Molecular Gas Content of LSB and HSB Galaxies

Figures 5 – 8 compare the results from this and all other LSB galaxy CO studies with a sample of measurements from a variety of other galaxy studies. These include 'standard' HSB disk galaxy studies (Boselli, et.al 1996; Casoli, et.al 1996), dwarf galaxy studies (Tacconi & Young 1987), and a study of extreme late-type spiral galaxies (Matthews & Gao 2001). In all cases a conversion factor of $N(H_2)/\int T(CO)dv = 3.6 \times 10^{20}$ cm^{-2}/(K km s^{-1}) was used to allow ready comparison between the results.

In all the CO non-detections in our survey, the upper limits placed on M_{H_2}/L_B are significantly lower than the upper limits found in previous LSB galaxy CO studies. However, examining the various plots (Figures 5 – 8) one can see that in the majority of cases the upper limits placed on M_{H_2} and M_{H_2}/M_{HI} in LSB galaxies are not unreasonably low when compared to the trends seen in the majority of other spiral galaxy studies. That is, although the LSB galaxies typically lie at the low M_{H_2} and M_{H_2}/M_{HI} end of the spectrum, the range of the data seen in the plots of M_{H_2} and M_{H_2}/M_{HI} versus M_B, W_{20}^{cor}, L_{FIR} and

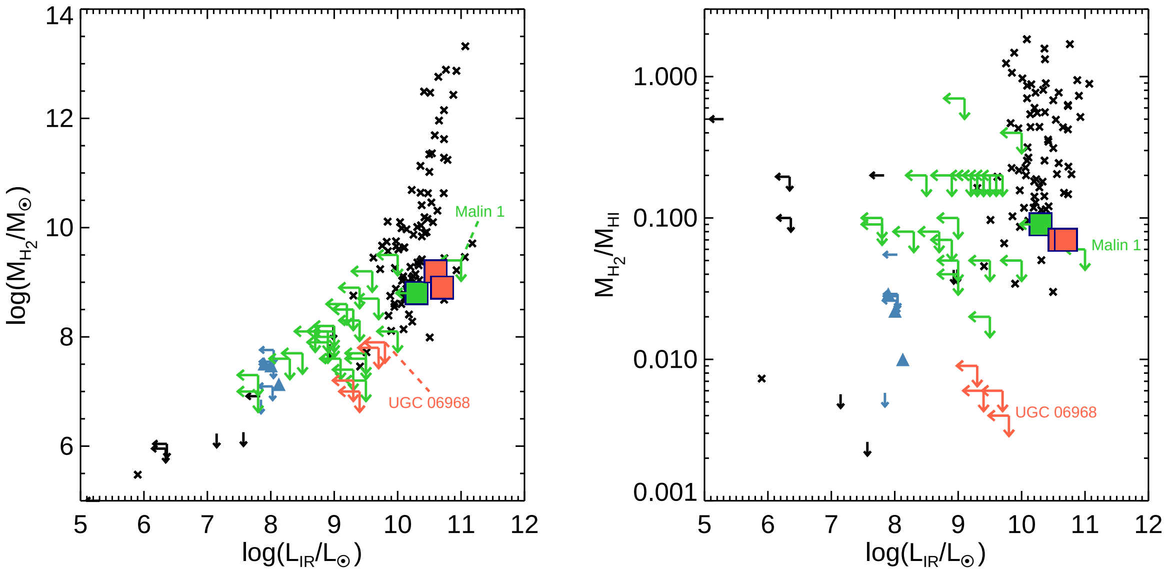

Fig. 7.— Infrared luminosity versus H_2 mass (left) and the H_2-to-H I mass ratio (right). The red symbols are LSB galaxies from this survey, the green symbols are LSB galaxy measurements from previous surveys (O'Neil, et.al 2003; Braine, Herpin, & Radford 2000; de Blok & van der Hulst 1998; Schombert, et.al 1990), the blue symbols are from the Matthews & Gao (2001) study of CO in extreme late-type spiral galaxies, and the black symbols are taken from various studies of the CO content in HSB spiral galaxies (Casoli, et.al 1996; Boselli, et.al 1996; Tacconi & Young 1987). An arrow indicates only an upper limit was found. Note that only the upper limits of L_{IR} were found for the LSB galaxies. Both Malin 1 and UGC 06968, the two massive LSB galaxies discussed in Section 5.3, are labelled on these plots.

morphological type for the HSB and dwarf galaxies covers the data points from the majority of the LSB galaxies. The three CO LSB galaxies also have M_{H_2} and M_{H_2}/M_{HI} values within the HSB galaxy range, but again lying at the low edge of the M_{H_2} and M_{H_2}/M_{HI} distribution as defined by HSB galaxies.

There are, though, two exceptions to this rule – UGC 06968 and Malin 1. Both have upper limits on M_{H_2} and $M_{H_2}/M_\odot$ well below that of other galaxies with the same velocity width, magnitude, and/or morphological type (Figures 5, 6, and 8). It is interesting to note that these galaxies are the only two LSB systems with masses and luminosities rivaling that of the three LSB galaxies with CO detections, as well as having similar optical emission lines and near-IR emission. These galaxies are further discussed in Section 5.3.

5. Star Formation and Molecular Gas in LSB Systems

5.1. Theories on the Efficacy of Forming Molecular Gas in LSB Galaxies

The previous lack of CO detection in LSB galaxies has been attributed to a number of different factors. One argument used to explain the low molecular gas content in LSB galaxies springs from the low metallicities commonly associated with LSB disks (de Blok

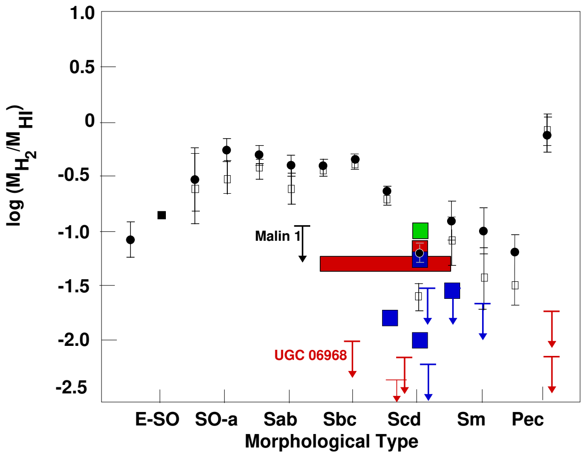

Fig. 8.— Variation of the molecular-to-atomic gas fraction along the morphological type sequence. The red symbols are the individual LSB galaxies in this survey, the green symbol is the one LSB galaxy detection from a previous survey (O'Neil, Hofner, & Schinnerer 2000). The size of the boxes represent the errors associated with our observations. The black symbols are taken from Casoli, et.al (1998), and are the mean values taken from a compendium of 582 CO observations of disk galaxies. The filled circles show mean values with upper limits treated as detections, and open squares give the mean values when upper limits are taken into account using a survival analysis method. The error bars in these points give the error on the mean. For comparison, the blue symbols are the individual extreme late-type galaxy sample of Matthews & Gao (2001). Both Malin 1 and UGC 06968, the two massive LSB galaxies discussed in Section 5.3, are labelled on these plots.

& van der Hulst 1998; McGaugh 1994). Low metallicities mean there will be a lack of dust grains to drive molecule formation, resulting in a low molecular-to-atomic gas ratio. Additionally, the dust grains provide shielding against the interstellar radiation field for the H_2 and CO molecules, again reducing the amount of molecular gas within the galaxies. Finally, as the CO molecule more readily photodissociates, the lack of dust grains will result in a lower CO-to-H_2 ratio and thus a higher CO-to-H_2 conversion factor (O'Neil, Hofner, & Schinnerer 2000; Mihos, Spaans, & McGaugh 1999; de Blok & van der Hulst 1998; Schombert, et.al 1990).

An alternative scenario used to explain the low CO fluxes found for LSB galaxies is to impose a truncated initial mass function (IMF) on a constant star formation rate (SFR) within LSB systems (Schombert, et.al 1990). This SFR could be adjusted to match the estimated amount of H_2 seen in LSB galaxies. Additionally, the IMF would have to be skewed to produce a high fraction of A and F stars and relatively few O and B stars. This would result in a reduction of the heavy element yield during the star formation process, lowering the overall molecular gas content of LSB galaxies.

Braine, Herpin, & Radford (2000) offered the argument that, at least within the environment of Malin 1 (and presumably similar LSB galaxies), the effects of metallicity on the CO-to-H_2 conversion factor are not enough to raise the molecular gas content to the amount expected based off the predicted

SFR. Instead, they argue that the gas (and dust) in Malin 1 is so cold as to reduce the CO emission from molecular clouds to a rate much less than that of our galactic disk. This would considerably reduce the CO emission per H_2 mass and, when combined with the metallicity effects, could be used to explain the low upper limit placed on the CO flux.

A final argument often invoked to explain the previous lack of CO detection within LSB galaxies results from the low baryonic column densities found within these systems (O'Neil, Hofner, & Schinnerer 2000; Mihos, Spaans, & McGaugh 1999; de Blok & van der Hulst 1998; Schombert, et.al 1990). First, the low dust column densities will, as mentioned earlier, result in a deficit of dust grains to act as a catalyst in the conversion of H I into H_2. Secondly, the diffuse ISM will result in less shielding against UV photons. Lastly, the low column densities result in a low overall SFR, reducing the metallicity of the system, with the effects mentioned above.

5.2. Comparing the Results with the Theories

For the first time we have available a catalog of over 30 CO measurements of LSB galaxies, including three detections. As a result we can compare the properties of the CO and non-CO LSB galaxies with the various theories given in the last section with the hope of understanding better the processes which govern molecular gas within LSB systems.

In Section 4.2 we determined that the factors which differentiate the CO LSB galaxies and the majority of the non-CO LSB galaxies are the galaxies' sizes, masses, and central bulges. (The two notable exceptions to this rule, UGC 06968 and Malin 1, will be discussed in the next subsection.) It seems likely that the presence of a central bulge within LSB galaxies is directly tied to the mass of the systems – the more massive a galaxy is, the larger its gravitational potential, and the more likely it will have a central mass concentration. This supposition is borne out with observation, as the majority of LSB galaxies known with $M_B < -19$ have bulges (Sprayberry, et.al 1995; Pickering, et.al 1997). The fact that the more massive LSB systems have a centrally concentrated region of high baryonic density means that within these galaxies' core the majority of arguments governing low CO and/or molecular gas content in the low density environment of LSB disks do not hold. Instead the central regions of these galaxies should undergo a similar star formation history to the core of a 'typical' HSB spiral galaxy, albeit with a slower gas infall rate. This idea is confirmed by the optical spectra we obtained of the three LSB galaxies with and without detected CO emission, as the three CO LSB galaxies have optical spectra indicative of a much older stellar population than is found for the three non-CO galaxies.

However, even including the three LSB galaxies with CO detections, it is clear that the CO content of LSB galaxies is lower than that found in an 'average' HSB spiral galaxy. That is, although both the measured values and upper limits show the CO content of LSB galaxies lie within the range set by HSB galaxies, the LSB systems lie on the low end of the HSB galaxy distribution range, but not so low as to set the LSB galaxies apart. Going through the possibilities laid out in Section 5.1, it seems clear that the explanation for the lower CO fluxes found in LSB systems is directly related to the overall lower density intrinsic to LSBs. Within the pure disk LSB galaxies it is probable that the low upper limits placed on the CO flux is due both to a lower than average molecular gas content and to a CO-to-H_2 conversion factor which is higher than that found within, e.g. the Milky Way. Similarly, the lower CO fluxes found within the bulges of the more massive LSB galaxies are likely due to an low infall rate of gas feeding the star formation processes within the bulge, and a lower metal content within the infalling gas.

5.3. UGC 06968 and Malin 1

UGC 06968 and Malin 1 are remarkable for being two of the largest and most massive of the LSB galaxies studied. They are the only two LSB galaxies studied with $M_B < -21$ (the usual cut-off for classifying an LSB galaxy as a massive system – see, e.g. Pickering, et.al 1997). Additionally, they are two of only four galaxies with $M_{HI} > 10^{10}$ $M_\odot$ and $W^{HI}_{20_{cor}} > 550$ km s^{-1}. As it appears that only the massive LSB galaxies have detectable quantities of CO, it is worthwhile to ask the question of why, when CO was readily detected in the other three massive LSB systems, no molecular gas has been seen in either UGC 06968 or Malin 1.

Because of its distance ($v_{HEL} = 24733$ km s^{-1}), the upper limits placed on Malin 1's absolute CO flux measurement are not exceptionally low – $M_{H_2} < 10^{9.4}$ $M_\odot$ and $M_{H_2}/M_{HI} < 0.06$. Regardless, when compared with the H_2 masses found for other HSB and LSB galaxies of similar mass, Malin 1's upper limits indicate it has a molecular gas content below that found for all other galaxies of its size, mass, or magnitude. Additionally, Malin 1 has a surprisingly low value for L_{FIR} as measured by the IRAS upper limits (Table 2). Braine, Herpin, & Radford (2000) state that, based primarily off the low L_{FIR} values, the gas and dust in Malin 1 is quite cold, reducing the galaxy's CO-to-H_2 fraction. From this they conclude that the H_2 mass of Malin 1 is likely near that of similar spiral galaxies, and it is only the CO gas which is lacking.

Classified as an AGN/LINER system by Schombert (1998), UGC 06968 falls well off the expected range of values for both M_{H_2} and M_{H_2}/M_{HI}. Looking at Figures 5 and 6 we can see that the upper limit found for UGC 06968's H_2 mass is at least ∼10 times less than would be expected, while the galaxy's molecular-to-atomic mass ratio (M_{H_2}/M_{HI}) is only 5% that of two LSB galaxies with CO detections and similar global properties. Like Malin 1, which has a similar morphology and classification, UGC 06968 has a low L_{FIR} limit for its size, indicating it, too, may contain extremely cold gas and dust, reducing its CO flux and increasing its H_2-to-CO conversion factor. Unlike Malin 1, though, the upper limits placed on UGC 06968's CO flux are low enough that a low gas temperature alone cannot increase the galaxy's H_2-to-CO conversion factor enough to raise M_{H_2} up to the value found for similar HSB systems. Looking at the various models of Mihos, Spaans, & McGaugh (1999), the clearest means of increasing UGC 06968's H_2 mass to the lowest value found for any other galaxy with similar global properties is by reducing the metallicity of the galaxy's *bulge* to something near 1/5 the solar value. (In the Mihos, et.al models, the lower metallicities result in fewer C and O atoms from which to form CO. This increases the CO-to-H_2 conversion factor in a manner analagous to that found by, e.g. Wilson 1995, Israel 1997, and Maloney & Black 1988.) Even if this is done, though, the M_{H_2}/M_{HI} value for UGC 06968 will be half that found for galaxies with similar masses and luminosities. A second possibility is that, unlike UGC 01922, the CO gas within UGC 06968 may not be concentrated within its core but instead may be spread throughout the galaxy's disk. As the disk of UGC 06968 extends well beyond that of the IRAM beam, this would imply we observed only a small fraction of UGC 06968's total molecular gas. If this is the case, though, it still would not explain why UGC 06968's molecular gas distribution is so different from other galaxies with similar morphologies. As a result, it is more likely that our observations did include the majority of the molecular gas within the galaxy, and UGC 06968 is simply deficient in CO gas.

6. Conclusion

We have obtained seven new, deep CO observations of LSB galaxies. Combined with all previous CO observations taken of LSB systems, we have a total of 34 observations, in which only 3 galaxies have had detections of their molecular gas. Looking at the differences between both the CO and non-CO LSB galaxies and and a collection of HSB galaxies with CO observations indicates it is primarily the lower baryonic density intrinsic to LSB galaxies which is causing their low CO fluxes. As has been discussed in previous papers, this in turn is likely responsible both for a low CO-to-H_2 ratio within the galaxies and for a lower density of molecular gas within LSBs. As a result, it is only those LSB galaxies which contain regions of higher baryonic density, such as the high mass LSB galaxies with distinct central bulges, in which CO gas will be readily detectable.

It is interesting to note that two of the most massive LSB galaxies studied have upper limits placed on their CO fluxes well below that of similar LSB and HSB galaxies. In the case of Malin 1 the difference between the upper limits placed on the galaxy' CO gas can be largely explained through assuming a very low temperature for the galaxy's gas and dust (Braine, Herpin, & Radford 2000). In the case of UGC 06968, though, temperature alone cannot be used to explain the galaxy's low M_{H_2} and extremely low M_{H_2}/M_{HI} values. Instead we must resort to also assuming a very low metallicity within the galaxy's core and/or a much lower baryonic density even in the galaxy's central region than its optical morphology and AGN/LINER characteristics suggest.

Even though the majority of observations taken of LSB galaxies result in only upper limits on the galaxies' CO flux, we are gradually gaining a clearer picture of the ISM, and consequently the SFH of these enigmatic systems. As the theories and observations are continued, we should gain a much clearer understanding of the star formation processes within the low density environments of LSB galaxies.

Thanks to Greg Bothun for providing the PMO images of UGC 12289 and to Liese van Zee for help with taking and reducing the Palomar spectra. P.H. acknowledges partial support from the Puerto Rico Space Grant Consortium and from NSF grant EPS-9874782. This research has made use of the NASA/IPAC Extragalactic Database (NED) which is operated by the Jet Propulsion Laboratory, California Institute of Technology, under contract with the National Aeronautics and Space Administration.

REFERENCES

Bergvall, Nils, Rvnnback, Jari, Masegosa, Josefa, & Vstlin, Gvran 1999 A&A 341, 697

de Blok, W.J.G, & van der Hulst, J.W. 1998 A&A 336, 49D

de Blok, W.J.G, & McGaugh, S. 1997 MNRAS 290, 533

de Blok, W.J.G, McGaugh, S., & van der Hulst, J.W. 1996 MNRAS 283, 18

de Blok, W.J.G, van der Hulst, J.W., & Bothun, G. 1995 MNRAS 274, 235

Boselli, A., Mendes de Oliveira, C., Balkowski, C., Cayatte, V., Casoli, F. 1996 A&A 314, 738

Boselli, A. & Gavazzi, G. 1994 A&A 283, 12

Braine, J., Herpin, F., & Radford, S. J. E. 2000 A&A 358 494

Burkholder, V., Impey, C., & Sprayberry, D. 2001 AJ 122, 2318

(Buisson, et.al 2002).

Buisson, G., et.al (2002) *CLASS Continuum and Line Analysis System Handbook*, online at http://iram.fr/GS/class/class.html

Casoli, F., Sauty, S., Gerin, M., Boselli, A., Foqué, P., Braine, J., Gavazzi, G., Lequeux , J., & Dickey, J. 1998 A&A 331, 451

Casoli, F., Dickey, J., Kazes, I., Boselli, A., Gavazzi, G., Jore, K. 1996 A&AS 116, 193

Davies, J. I., Phillipps, S., & Disney, M. J. 1990 MNRAS 244, 385

Eder, J. & Schombert, J. 2000 ApJS 131, 47

Garnier, R. Paturel, G., Petit, C., Marthinet, M. C., & Rousseau, J. 1996 A&AS 117, 467

Gavazzi, G. 1987 ApJ 320, 96

Giovanelli, R. & Haynes, M. 1985 AJ 90, 2445

Howarth, I. 1983 MNRAS 203, 801

Huchtmeier, W.K., Karachentsev, I.D., & Karachentseva, V.E. 2000 A&AS 147, 187

van der Hulst, J. M., Skillman, E. D., Smith, T. R., Bothun, G. D., McGaugh, S. S., & de Blok, W. J. G. 1993 AJ 106, 54

Impey, C. & Bothun, G. 1989 ApJ 341, 89

Isreal, F. 1997 A&A 328, 471

Kutner, M. L. & Ulich B. L. 1981, ApJ 250 341

Maloney, P., & Black, J. H. 1988, ApJ 325, 389

Massey, Philip, Strobel, Kevin, Barnes, Jeannette V., & Anderson, Edwin 1988 ApJ 328, 315

Matthews, L. & Gao, Y. 2001 ApJ 549, L191

Mihos, C., Spaans, M., & McGaugh, S. 1999 ApJ 515, 89

McGaugh, S. & Bothun, G. 1994 AJ 107, 530

McGaugh, S. 1994 ApJ 426, 13

Nilson, P. 1973 *Uppsala General Catalogue of Galaxies* Uppsala Astronomiska Observatoriums Annaler (Uppsala: Astronomiska Observatorium)

O'Neil, K., Bothun, G., van Driel, W., & Monnier-Ragaigne, D. 2003, preprint

O'Neil, K. & Schinnerer, E. 2003, preprint

O'Neil, K., Hofner, P., & Schinnerer, E. 2000 ApJ 545, L99

O'Neil, K., Bothun, G., & Schombert, J. 2000 AJ 119, 136

O'Neil, K., Bothun, G., & Cornell M. 1997a AJ 113, 1212

O'Neil, K., Bothun, G., Schombert, J., Cornell, M., & Impey C. 1997b AJ 114, 2448

Oke, J. & Gunn, J. 1983 ApJ 266, 713

Oke 1990, AJ 99, 1621

Pickering, T.E., Impey, C.D., van Gorkom, J.H., & Bothun, G.D. 1997 AJ 114, 1858

Pildis, R., Schombert, J., & Eder, J. 1997 ApJ 481, 157

Roennback, J. & Bergvall, N. 1995 A&A 302, 353

Sanders, D., Scoville, N., Young, J., Soifer, B., Schloerb, F., Rice, W., & Danielson, G. 1986 ApJ 305, L45

Schlegel, D., Finkbeiner, D., & Davis, M 1998 ApJ 500, 525

Schombert, J., Bothun, G., Schneider, S., & McGaugh, S. 1992 AJ 103, 1107

Schombert, J., Bothun, Gregory D., Impey, Chris D., & Mundy, Lee G. 1990 AJ 100, 1523

Schombert, J. 1998 AJ 116, 1650

Schombert, J. & Bothun, G. 1988 AJ 95, 1389

Seaton, M. 1979 MNRAS 187, 73

Sprayberry, D., Impey, C.D., Bothun, G.D., & Irwin, M.J. 1995 AJ 109, 558

Tacconi, L. & Young, J. 1987 ApJ 322, 681

van Zee, L., Salzer, J., Haynes, M., O'Donoghue, A., & Balonek, T. 1998 AJ 116, 2805

Wilson, C. D. 1995, ApJ 448, L97

Young, J. et.al 1995 ApJS 98, 219

This 2-column preprint was prepared with the AAS LaTeX macros v5.0.

TABLE 3
CO PROPERTIES OF ALL LSB GALAXIES OBSERVED AT CO

Galaxy	Line	$\int T_{MB} dv$† [K km s^{-1}]	v_{HEL} [km s^{-1}]	Width [km s^{-1}]	$\log(M_{H_2}/M_{\odot})$‡	M_{H_2}/M_{HI}
UGC 01922	1−0	1.38	10795	404	9.2	0.07
UGC 01922	2−1	2.96	10802	403	8.9	0.04
UGC 12289	1−0	1.16	10162	200	9.0	0.07
UGC 12289	2−1	0.69	10185	201	8.2	0.01
			Previous Detection			
[OBC97] P06-1[1]	1−0	0.95	10904	302	8.8	0.09
[OBC97] P06-1[1]	2−1	1.14	10903	216	8.3	0.03
			Non-detections - This Paper			
[OBC97] P07-1	1−0	<0.13	···	···	<7.0	<0.006
[OBC97] P07-1	2−1	<0.032	···	···	<5.7	<0.003
[OBC97] N09-2	1−0	<0.18	···	···	<7.8	<0.006
[OBC97] N09-2	2−1	<0.33	···	···	<7.5	<0.003
[OBC97] P05-6	1−0	<0.22	···	···	<7.2	<0.009
[OBC97] P05-6	2−1	<0.39	···	···	<6.9	<0.005
[OBC97] C04-1	1−0	<0.37	···	···	<8.1	<0.02
[OBC97] C04-1	2−1	<0.88	···	···	<7.9	<0.01
UGC 06968	1−0	<0.21	···	···	<7.9	<0.004
UGC 06968	2−1	<0.58	···	···	<7.8	<0.003
			Previous Non-Detections			
LSBC F575-3[2]	1−0	<0.14	···	···	<6.1	<0.05
LSBC F571-V2[2]	1−0	<0.19	···	···	<7.0	<0.09
LSBC F638-3[2]	1−0	<0.22	···	···	<8.1	<0.2
LSBC F583-5[2]	1−0	<1.20	···	···	<7.9	<0.07
LSBC F651-2[2]	1−0	<0.22	···	···	<7.6	<0.08
LSBC F721-1[2]	1−0	<0.19	···	···	<8.7	<0.2
LSBC F571-V1[3]	2−1	<0.20	···	···	<7.6	<0.2
[OBC97] P05-5[1]	1−0	<0.12	···	···	<7.6	<0.7
[OBC97] P05-5[1]	2−1	<0.21	···	···	<7.3	<0.3
LSBC F636-1[2]	1−0	<0.30	···	···	<8.5	<0.2
LSBC F562-V2[2]	1−0	<0.33	···	···	<8.9	<0.2
LSBC F563-V1[3]	2−1	<0.28	···	···	<7.4	<0.2
LSBC F561-1[1]	1−0	<0.93	···	···	<8.3	<0.2
LSBC F574-10[2]	1−0	<0.46	···	···	<7.3	<0.1
LSBC F585-V1[2]	1−0	<1.17	···	···	<7.7	<0.2
[OBC97] C04-2[1]	1−0	<0.096	···	···	<7.2	<0.02
LSBC F563-V2[2]	1−0	<0.42	···	···	<8.6	<0.2
LSBC F563-1 [2]	1−0	<0.53	···	···	<8.0	<0.05
LSBC F571-5[2]	1−0	<0.35	···	···	<8.5	<0.2
[OBC97] C05-3[1]	1−0	<0.14	···	···	<8.1	<0.05
LSBC F585-3[2]	1−0	<0.66	···	···	<8.1	<0.04
LSBC F568-V1[3]	2−1	<0.19	···	···	<7.7	<0.05
LSBC F583-1[2]	1−0	<0.49	···	···	<8.1	<0.08
LSBC F582-V1[2]	1−0	<0.47	···	···	<9.5	<0.4
LSBC F564-V2[1]	1−0	<0.70	···	···	<8.2	<0.1
LSBC F582-2[2]	1−0	<0.54	···	···	<9.2	<0.2
Malin 1[4]	1−0	<0.15	···	···	<9.4	<0.06
Malin 1[4]	2−1	<0.35	···	···	<8.7	<0.01

TABLE 3—*Continued*

Galaxy	Line	$\int$ T$_{MB}$dv† [K km s^{-1}]	v$_{HEL}$ [km s^{-1}]	Width [km s^{-1}]	log(M$_{H_2}$/M$_\odot$)‡	M$_{H_2}$/M$_{HI}$

NOTE.—†Non-detection limits are $I_{CO} < 3T_{MB}\frac{v_{HI}^{20}}{\sqrt{N}}$ (N = the number of channels, T$_{MB}$ is the 1σ rms main beam temperature).
‡As described in Section 3, conversion to M$_{H_2}$ was done using N(H$_2$)/$\int$ T(CO)dv = 3.6×10^{20} cm^{-2}/(K km s^{-1})

REFERENCES.—[1]O'Neil, Hofner, & Schinnerer (2000); [2]Schombert, et.al (1990); [3]de Blok & van der Hulst (1998); [4]Braine, Herpin, & Radford (2000)

TABLE 4

OBSERVED OPTICAL LINES

Galaxy	Hβ EW	Hβ flux	O II [λ3727] EW	O II [λ3727] flux	Ca II(K) [λ3934] EW	Ca II(K) [λ3934] flux	H7+Ca II(H) [λ3969] EW	H7+Ca II(H) [λ3969] flux	G band [λ4306] EW	G band [λ4306] flux
[OBC97] C04-2	8.0	2.9	27	12	···	···	···	···	···	···
[OBC97] P05-5	···	···	···	···	···	···	···	···	···	···
[OBC97] P05-6	···	···	9.0	9.1	···	···	···	···	···	···
[OBC97] P06-1	-4.0	-3.4	4.1	3.7	-8.2	-6.1	-12	-8.8	···	···
UGC 01922	3.2	19	9.0	16	-8.8	-13	-6.1	-11	-4.2	-25
UGC 12289	···	···	···	···	-8.3	-3.2	-8.1	-3.5	-5.3	-3.4

NOTE.—All errors are within 15%. EW is in Å. Flux is in units of 10^{-16} erg s^{-1} cm^{-2} Å^{-1}. Values reported as negative are in absorption.

TABLE 4

OBSERVED OPTICAL LINES, *cont*

Galaxy	Na I [$\lambda\lambda$5889,5895] EW	Na I flux	Hα [λ6563] EW	Hα flux	N II [$\lambda\lambda$6548,6583] EW	N II flux	S II [$\lambda\lambda$6717,6731] EW	S II flux	c
[OBC97] C04-2	···	···	40.	13.	6.0	2.1	20.	7.0	0.52
[OBC97] P05-5	···	···	3.7	0.63	···	···	1.8	0.30	···
[OBC97] P05-6	···	···	11.	8.5	···	···	2.9	1.9	···
[OBC97] P06-1	-2.5	-3.6	3.1	5.5	2.1	3.8	2.7	6.2	···
UGC 01922	-4.8	-41	91.	120	130	170	140	190	0.36
UGC 12289	-3.3	-5.4	4.5	6.7	6.2	11.	2.0	2.9	···

NOTE.—All errors are within 15%. EW is in Å. Flux is in units of 10^{-16} erg s^{-1} cm^{-2} Å^{-1}. Values reported as negative are in absorption. The reddening coefficient c=1.28E($B-V$). *Note that if no reddening coefficient is given, the data is uncorrected for Extragalactic extinction.*